Reaction efficiency of diffusion-controlled processes on finite, planar arrays. II. Crystal surfaces

John J. Kozak,[1,*,†] Jack Brzezinski,[2,*,‡] and Roberto A. Garza-López[3,*,§]
[1]*Department of Chemistry, DePaul University, 243 South Wabash Avenue, Chicago, Illinois 60604, USA*
[2]*AHA Communications Inc., 151 Michigan Avenue, Chicago, Illinois 60601, USA*
[3]*Seaver Chemistry Laboratory and Department of Chemistry, Pomona College, Claremont, California 91711, USA*
(Received 19 March 2009; published 20 August 2009)

We consider 36 planar nets identified by O'Keeffe and Hyde and calculate for each, using the theory of finite Markovian processes, the overall mean walk length $\langle n \rangle$ (first passage time) of a reactant diffusing randomly on a finite platelet before being trapped at a reaction center; the results are analyzed in terms of the total number N of lattice sites, the number N_b of boundary sites, the average valence $\bar{\nu}$, and the bond orientation function Ψ. We establish that crystalline platelets that are members of the same compatible class are characterized by very comparable catalytic efficiencies. The results obtained are also linked to an analysis of the kinetics of docking in postnucleation stages of protein self-assembly and to a recent conjecture on the symmetries of planar nets and the hard disk freezing transition.

DOI: 10.1103/PhysRevE.80.021116 PACS number(s): 05.40.Fb, 05.20.−y, 68.35.Fx, 02.50.Ey

I. INTRODUCTION

In a previous contribution [1] we investigated the reaction efficiency of diffusion-controlled processes on finite, planar arrays having chemical or physical receptors. Interest in this problem is driven by several factors among which are the following. First, few physical systems are characterized by perfectly ordered infinite arrays free of imperfections; imperfections bifurcate the space into domains or regions of finite spatial extent. Second, it has long been recognized that reactions carried out in/on organized molecular assemblies can be kinetically advantaged relative to reaction in homogeneous solution [2]. And, most importantly, techniques now widely used in nanotechnology have been used to fabricate compartmentalized systems of specific geometry and consequent functionality. These factors warrant a detailed study of the influence of finite-system geometries on the efficiency of chemical and physical processes.

In [1], the theory of finite Markovian processes was mobilized to calculate the site-specific average walk length $\langle n \rangle$ of a particle undergoing random displacements on small lattices before localization (trapping); see also the review [3]. By analyzing the (numerically exact) results obtained on lattices of finite extent having boundaries of arbitrary shape, definite conclusions could be drawn on the separate influence on the reaction efficiency of system size N, boundary (or perimeter) sites N_b, and average valence $\bar{\nu}$, as well as the root-mean-square distance of the N lattice sites relative to the center of the array. Comparison of the results obtained with predictions based on analytical expressions derived by Montroll and Weiss [4] in their classic studies on infinite periodic lattices of uniform valence [viz., on the hexagonal (ν=3), square-planar (ν=4) and triangular (ν=6) lattices] revealed a more subtle dependence on the lattice parameters N and ν and a further pronounced dependence on the geometrical shape of the domain, as we shall now review.

The finite triangular, square-planar, hexagonal, and Penrose lattices considered in [1] were designed to assess the extent to which the known analytical dependence of $\langle \bar{n} \rangle$ on N and ν for infinite periodic lattices [3] was modulated when finite lattices were considered. Three general conclusions were drawn. First, for fixed N, the smaller the number N_b of vertices defining the boundary of the finite lattice under consideration, the smaller the value of $\langle \bar{n} \rangle$ of the random walker before trapping. Second, for fixed N and fixed N_b, the smaller the value of the overall (average) root-mean-square distance $(\bar{r}^2)^{1/2}$ of the N lattice sites relative to the center of the array, the smaller the value of $\langle \bar{n} \rangle$. Third, for fixed N, N_b, and root-mean-square distance, $\langle \bar{n} \rangle$ decreased with an increase in the (overall) average valence $\bar{\nu}$ of lattice sites comprising the array.

The conclusions cited in the preceding paragraph were the basis of a proposal put forward in [5] that the kinetics of docking in the postnucleation stages of protein, and zeolite self-assembly might be understood in terms of a "corresponding states" approach. In particular, it was conjectured there (but not proved) that a topological (diffeomorphic) distortion of a template surface, one that maintained constant the values of N, N_b, and $\bar{\nu}$, should preserve the qualitative trends in the site-specific docking efficiency exhibited by the precursor surface.

The study undertaken here is designed to explore quantitatively this corresponding states idea by using templates that describe known planar nets in crystal chemistry, viz., alloys or inorganic solids whose network structure has been thoroughly characterized. The following section develops the basic idea using two examples illustrated in [6]. Section III provides a compilation of results obtained using the theory of Markovian processes to investigate 30 of the planar nets identified by O'Keeffe and Hyde. The concluding section (Sec. IV) summarizes our results using both the geometrical metrics noted above and the bond orientation function Ψ, which is now standard in describing glassy materials, disordered solids, and the hexatic phase in the Kosterlitz, Thou-

*Corresponding authors.
†kozak@depaul.edu
‡brzezinski_j@yahoo.com
§rgarza@pomona.edu; http://pages.pomona.edu/~ragl4747

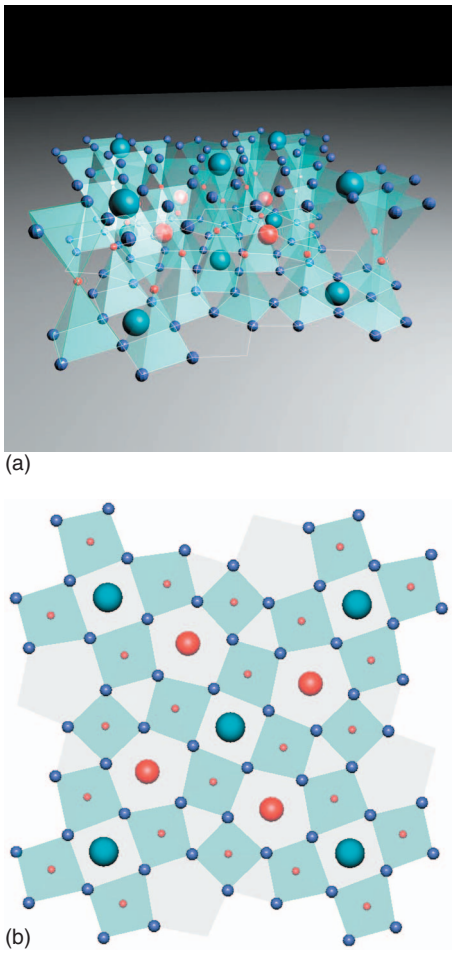

FIG. 1. (Color) (a) Tetragonal tungsten bronze $K_3W_5O_{15}$ (side view). (b) Tetragonal tungsten bronze (top view).

less, Halperin, Nelson, and Young (KTHNY) theory [7–11] of the hard disk phase transition. We close by relating the results reported here to a recent study [12] which identified tessellations that believed to be signatures of symmetries important in the hard disk transition.

II. COMPATIBLE NETS

The point of departure for the study presented in [6] was the idea that crystal structures could be considered as stackings of two-dimensional packings of atoms ("layers"). Thus, for example, tetragonal tungsten bronze (Fig. 1) when viewed in this way has the layer structure illustrated in Fig. 2. In O'Keeffe and Hyde's study this layer is labeled net 21; for the reader's convenience, in this example, as in all the examples considered later in this work, we shall use the net designation presented in [6].

The nets considered in [6] were organized into two principal compatibility classes: the first based on the square-planar symmetry and the second based on the hexagonal system. Their net classification system was specified using two organizing relationships; for the square system,

$$N = A(p^2 + q^2),$$

and for the hexagonal system,

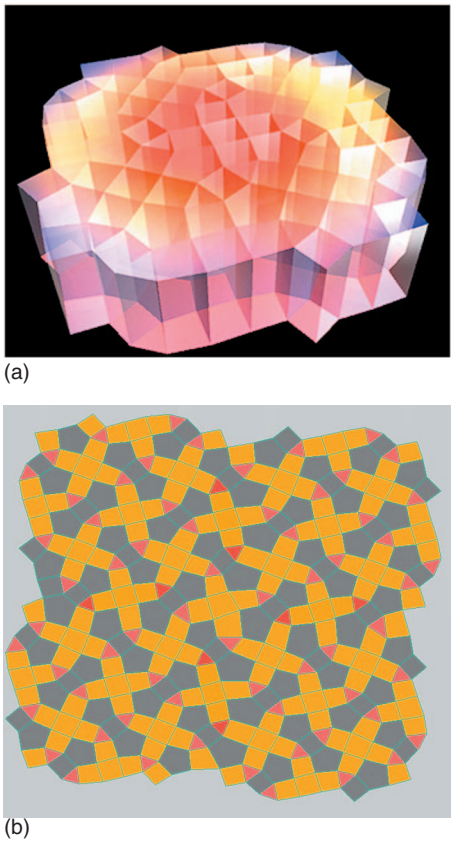

FIG. 2. (Color) (a) Projection highlighting the surface of $K_3W_5O_{15}$. (b) The planar net 21 (see text).

$$N = B(p^2 + pq + q^2),$$

where $[p,q]$ are integers and A or B are nonzero integers that are the same for two compatible nets. The consequences of this classification scheme were made explicit in their Table 2. All but four of the first 27 nets considered in [6] fall into one or the other of these classes.

The first (and simplest) example of a transformation between two lattices in the same compatibility class is illustrated in their Fig. 34 and displayed here in Fig. 3. The rotation of square groups of atoms which take the square-planar system, $[4^4]$, into the net, $[3^2\cdot4\cdot3\cdot4]$, is shown explicitly; in the notation of [6], these Schafli designations are labeled nets 2 and 6, respectively.

As is evident, the vertices of the nets displayed in Figs. 3 have been differentiated. Described now is the convention

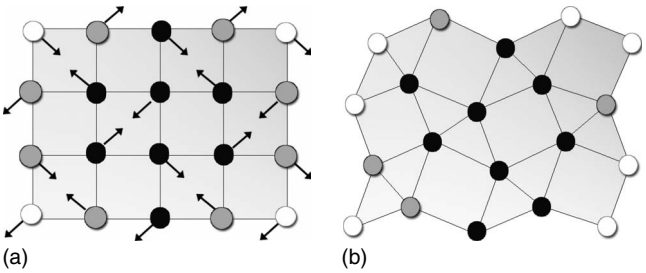

FIG. 3. (a) The precursor lattice $[4^4]$. (b) The planar net 6 $[3^2\cdot4\cdot3\cdot4]$.

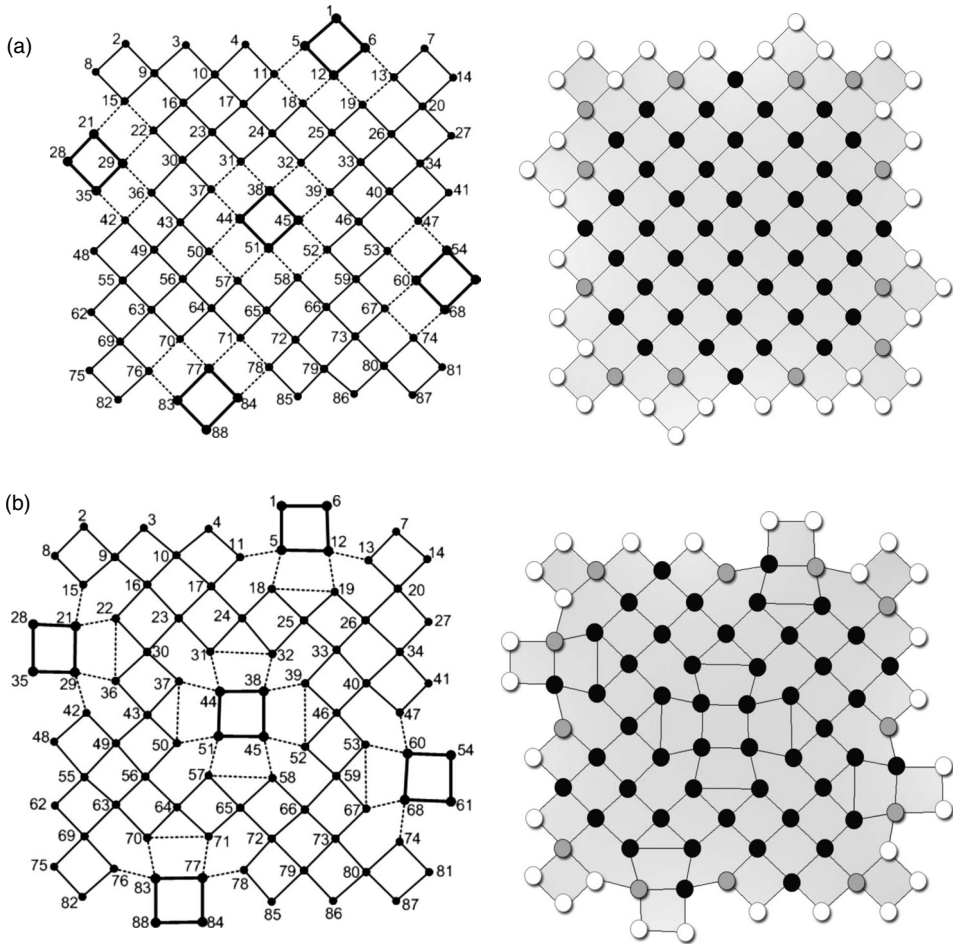

FIG. 4. (a) Square lattice $[4^4]$ Precursor. (b) Net 21.

used in coding the vertices in Fig. 3, which is the same convention that will be followed for all the other nets illustrated in this study. In the theory of finite Markovian processes, one places a "trap" (reaction center, active site) at a particular site (vertex i) on the lattice and then computes the average number $\langle n\rangle_i$ of steps before the random walker is localized (or "trapped"). For the particular site i, $\langle n\rangle_i$ is a measure of reaction efficiency at that site (relative to all other sites of the lattice). To obtain a metric for the platelet as a whole, one must compute $\langle n\rangle_i$ for all N sites of the given lattice and construct the overall average $\langle \bar{n}\rangle$.

The coding displayed in Figs. 3 then has the following description. Computing the site-by-site ratio

$$R = \frac{\langle n\rangle_i}{\langle \bar{n}\rangle}$$

if $\langle n\rangle_i$ is within 10% of the average value $\langle \bar{n}\rangle$, this site is represented by a filled gray circle; site values which are less than 90% of the mean value are designated by filled black circles and sites greater than 110% of the mean are given by open circles. Qualitatively, then, filled black circles represent sites of optimal catalytic activity and sites coded by open circles represent sites of marginal or poor catalytic activity.

We have performed calculations to characterize the catalytic activity for each of the platelets considered in this study. Displayed in the Appendix are 27 planar nets (redrawn from O'Keeffe and Hyde) with each site for each platelet coded using the above convention. The obtained values for the ratio R upon which these figures are based are presented in the supplementary online material [13].

As is already apparent from the coding in Fig. 3, and consistent with one's intuition, the optimal sites of catalytic activity for a platelet are in the "interior" whereas less effective sites are on the "boundary." This behavior is also seen in Fig. 4 which displays a second lattice $[5\cdot4^2, 5\cdot4\cdot3\cdot4, 5\cdot4^3, (5\cdot4\cdot3\cdot4)^2]$ derivable from $[4^4]$; the former is net 21 [see Fig. 39a in [6] and Figs. 1 and 2 above] and the second is, again, net 2.

We come now to the main point addressed in this paper. For nets that are in the same compatibility class, and derivable one from the other via elementary topological transformations, we examine how close are the calculated values of $\langle \bar{n}\rangle$ for compatible nets.

Examining Fig. 3, note that both nets are characterized by $N=20$, $N_b=16$; the overall average valence $\bar{\nu}$ for the finite $[4^4]$ net is 3.100 and for $[3^2\cdot4\cdot3\cdot4]$ the value is 3.700. The value of $\langle \bar{n}\rangle$ for the square net is 34.202, and for the second net the value is 33.846, with a difference of $\sim$1%. As will be discussed in Sec. IV, this ordering of the values of $\langle \bar{n}\rangle$ is consistent both with the predictions of the analytical asymptotic expressions derived by Montroll and Weiss [4]

TABLE I. Comparison of companion pairs of finite nets.

Net	N	N_b	$\bar{\nu}$	$\langle n \rangle$	Square net	$\bar{\nu}$	$\langle n \rangle$
6	36	20	4.00	69.921	6×6	3.33	71.280
19	49	24	3.43	110.412	7×7	3.43	104.150
21	64	36	3.38	158.808	4×16	3.38	209.318
Net	N	N_b	$\bar{\nu}$	$\langle n \rangle$	Hex net	$\bar{\nu}$	$\langle n \rangle$
7	40	24	3.33	97.182	4×10	4.65	87.384
11	64	36	4.78	211.412	8×8	4.78	185.481
3	30	22	2.53	70.543	3×10	4.33	69.507
4	48	24	4.38	105.731	6×8	4.88	95.831
8	48	24	3.58	110.627	6×8	4.88	95.831
Net	N	N_b	$\bar{\nu}$	$\langle n \rangle$	Square net	$\bar{\nu}$	$\langle n \rangle$
13	49	24	4.16	102.925	7×7	3.43	104.149
Net	N	N_b	$\bar{\nu}$	$\langle n \rangle$	Hex net	$\bar{\nu}$	$\langle n \rangle$
					7×7	4.90	97.775
Net	N	N_b	$\bar{\nu}$	$\langle n \rangle$	Square net	$\bar{\nu}$	$\langle n \rangle$
25	40	24	3.30	88.866	4×10	3.25	96.346
					Hex net	$\bar{\nu}$	$\langle n \rangle$
					4×10	4.65	87.384

for infinite periodic lattices and with the study of finite planar nets reported in [1]; in particular, with all other things being equal, the larger the value of the valence, the smaller the resulting $\langle \bar{n} \rangle$.

As a second example (Fig. 4), the square lattice has $N=88$, $N_b=44$, and $\bar{\nu}=3.455$, and net 21 has $N=88$, $N_b=48$, and $\bar{\nu}=3.364$. For the former finite net, $\langle \bar{n} \rangle = 223.388$, and for the second one, $\langle \bar{n} \rangle = 236.604$. As noted earlier, for finite platelets, for a given N, the value of $\langle \bar{n} \rangle$ is next governed by the value of N_b; here, the smaller N_b for the square-planar net leads to a somewhat smaller value of $\langle \bar{n} \rangle$. The difference noted, however, remains small, $<6\%$.

As these two examples demonstrate, nets of a given N which are members of the same compatibility class have "nearly" the same values of $\langle \bar{n} \rangle$, with the difference attributable to (slightly) different values of N_b and $\bar{\nu}$. This congruence is the basis of the idea of corresponding states in chemical catalysis that we posited at the outset of this study.

As a further illustration of this congruence, one can construct square-planar or hexagonal lattices which can be placed in correspondence with certain nets in the O'Keeffe and Hyde classification system. Specifically, one can design companion pairs of lattices with the same N and N_b (similar to the program that was carried out in [1]) and compare the values calculated for $\langle \bar{n} \rangle$. This correspondence is not "perfect" because, in pinning the values $[N,N_b]$, the geometry of the companion square-planar/hexagonal platelets becomes much more asymmetrical than the net being considered, and one knows from the study presented in [1] that the root-mean-square distribution of the N sites of the array relative to a centrosymmetric site is an important predictor in influencing the reaction efficiency. Having that said, the results of these comparisons are displayed in Table I. Note that we can also construct lattice comparisons for two of the four nets identified in [6] that are not easily classified in either the square or hexagonal systems (viz., nets 13 and 25). A glance at the results in this table shows that the quantitative differences between all companion pairs of lattices, taken together, average to $\sim 10\%$.

III. COMPILATION OF RESULTS

Listed in Table II are results for 27 of the nets identified in [6]. Reported here are the O'Keeffe and Hyde net number; the Schafli designation for each; the values of N, N_b, and $\bar{\nu}$ for the finite platelet considered; the packing fraction η for the unit cell; and the overall average mean walk length $\langle \bar{n} \rangle$, computed as described in Sec. II. As mentioned earlier, the values of the site-specific $\langle n \rangle_i$ and the overall $\langle \bar{n} \rangle$ are numerically exact; see [3]. Not included here, but given explicitly in [6], are examples (alloys and inorganic solids) drawn from the crystallographic literature of (almost) every net described in their study.

In addition to the above geometric signatures, we list in Table III the bond orientation parameter for most nets in the square and the hexagonal systems. For a reference triangular lattice, the parameter Ψ is defined as

TABLE II. Platelet characteristics and mean walk length.

Net	Schlafli	N	N_b	$\bar{\nu}$	η [a]	$\langle n \rangle$
	Square system ($A=1$)					
2	$[4^4]$	25	16	3.20	0.785398	45.071
6	$[3^2 \cdot 4 \cdot 3 \cdot 4]$	36	20	4.00	0.841787	69.921
9	$[4 \cdot 8^2]$	48	34	2.71	0.539012	144.169
19	$[5^4 \cdot 3^2 \cdot 5^2, (3 \cdot 5 \cdot 4 \cdot 5)^2, 3^2 \cdot 5^2]$	49	24	3.43	0.785398	110.412
20	$[(3 \cdot 5 \cdot 4 \cdot 5)^2, 3 \cdot 5 \cdot 3 \cdot 5]$	59	32	3.39	0.679012	143.985
21	$[5 \cdot 4^3, 5 \cdot 4 \cdot 3 \cdot 4, 5 \cdot 4^3, (5 \cdot 4 \cdot 3 \cdot 4)^2]$	64	36	3.38	0.677469	158.808
	Square system ($A=2$)					
12	$[3^3, (3 \cdot 4 \cdot 3 \cdot 4)^2]$	65	31	4.28	0.841787	145.202
14*	$[3 \cdot 6 \cdot 3 \cdot 6, (3^2.6^2)^2]$	33	31	3.39	0.680175	74.082
18	$[(5^3)^2, 5^4, 5^3, 5^4]$	51	28	2.90	0.709083	123.396
26	$[(4 \cdot 7^2)^2, (7^3)^2, (4 \cdot 7^2), 7^3]$	54	32	2.67	0.606655	158.808
	Hexagonal system ($B=1$)					
1	$[3^6]$	25	16	4.48	0.906900	44.668
7	$[3 \cdot 6 \cdot 3 \cdot 6]$	40	24	3.33	0.680175	97.182
11	$[4 \cdot 6 \cdot 12]$	64	36	2.69	0.486067	211.412
16(a)	$[(3^2 \cdot 4 \cdot 3 \cdot 4)^2, (3 \cdot 4 \cdot 6 \cdot 4)^2]$	62	28	3.84	0.781350	147.325
16(b)	$[(3^3 \cdot 4^2)^2, (3 \cdot 4 \cdot 6 \cdot 4)^2]$					149.737
17		76	32	4.00	0.789447	179.806
17*[b]		80	32	4.40	0.845836	178.239
23	$[(3 \cdot 4 \cdot 5 \cdot 4)^2, (3 \cdot 5 \cdot 4 \cdot 5)^2]$	54	30	3.33	0.715037	131.926
27	$[9^3, (3 \cdot 9^2)^2, 9^3, (3 \cdot 9^2)^2, 9^3, (3 \cdot 9^2)^2]$	38	27	2.53	0.750040	115.713
	Hexagonal system ($B=2$)					
3	$[6^3]$	30	22	2.53	0.604600	70.543
4	$[3^4 \cdot 6]$	48	24	4.38	0.777343	105.731
8	$[3 \cdot 4 \cdot 6 \cdot 4]$	48	24	3.58	0.729009	110.626
10	$[3 \cdot 12^2]$	48	38	2.71	0.390675	185.024
	Hexagonal system ($B=3$)					
22	$[(5^3 \cdot 3)^2, 5^3, 5^3 \cdot 3, 5^3]$	35	28	2.86	0.5771	85.565
24	$[3 \cdot 5 \cdot 3 \cdot 5, (3.4.5^2)^2]$	52	27	3.42	0.744 522	121.009
	Unassigned					
5	$[3^3 \cdot 4^2]$	52	25	4.38	0.841787	112.269
13	$[(3^3 \cdot 4^2)^2, (3^2 \cdot 4 \cdot 3 \cdot 4)^2]$	49	24	4.16	0.841787	102.925
15	Kagome tiling	60	30	3.30	0.665060	155.049
25	$[3 \cdot 4 \cdot 5 \cdot 4, (3 \cdot 4 \cdot 5^2)^2]$	40	24	3.40	0.751037	88.866

[a]Packing fraction calculated for the unit cell of the given net.

[b]Net 17* is described, but not illustrated, in [6]; it is net 17 with four additional vertices placed at the center of each of the four hexagons. As noted in [6], this net is of interest because it is the densest net with square symmetry.

$$\Psi = \frac{1}{N}\sum_{i=1}^{N} \frac{1}{N_{ij}} \sum_{j} e^{i6\theta_i}. \tag{1}$$

Here, N is the number of vertices (or "sites") in the unit cell; θ is the angle between the bond connecting particles i and j and an arbitrary, but fixed, reference axis; and the sum on j is over the N_{ij} nearest neighbors of i. For a square-planar reference lattice i, "6" in the above expression is replaced with "4." This parameter Ψ is useful in characterizing the hexatic phase in a $d=2$-dimensional system of hard disks, glassy

TABLE III. Valence and bond orientation parameters for unit cell and platelet (S=square system; H=hexagonal system; U=unassigned).

	Unit cell			Platelet		
Net/system	ν	Ψ_4	Ψ_6	ν^*	Ψ_4^*	Ψ_6^*
2/S	4	1.000	0.000	3.20	1.000	0.160
6/S	5	0.250	0.250	4.00	0.352	0.255
9/S	3	1.000	0.333	2.71	0.528	0.236
19/S	4	0.615	0.615	3.43	0.640	0.680
20/S	4	0.654	0.750	3.39	0.562	0.529
21/S	4	0.809	0.238	3.38	0.100	0.378
12/S	5	0.267	0.333	4.28	0.234	0.407
14*/S	4	0.250	1.000	3.39	0.331	1.000
18/S	3.56	0.667	0.393	3.56	0.537	0.670
26/S	3	0.333	0.556	3	0.285	0.546
1/H	6	0.000	1.000	4.48	0.174	1.000
7/H	4	0.500	1.000	3.33	0.520	1.000
11/H	3	0.577	0.333	2.69	0.587	0.229
16/H	4.38	0.388	0.075	3.84	0.408	0.140
17/H	4	0.116	0.100	4.00	0.440	0.184
17*/H	5	0.175	0.300	4.40	0.234	0.285
23/H	4	0.621	0.272	3.33	0.326	0.400
27/H	3	0.000	0.500	2.53	0.026	0.421
3/H	3	0.000	1.000	2.53	0.233	1.000
4/H	5	0.200	1.000	4.38	0.150	1.000
8/H	4	0.500	0.000	3.58	0.514	0.139
10/H	3	0.000	0.333	2.71	0.208	0.472
24/H	4	0.556	0.458	3.42	0.588	0.439
5/U	5	0.250	0.500	4.38	0.602	0.465
13/U	5	0.265	0.500	4.16	0.382	0.466
15/U	3.82	0.234	1.000	3.30	0.439	1.000
25/U	4	0.556	0.458	3.40	0.588	0.439

materials, and disordered solids (see Binder and Kob [14]) and is especially useful here in providing an independent metric for finite arrays of mixed valence.

Before reviewing the results in Table III, we comment briefly on the calculation of Ψ. For the unit cell of an infinite periodic lattice, e.g., for the square-planar net 2 or the triangular net 1, the calculation of Ψ is straightforward; for the square-planar system, net 2, Ψ_4 is 1 and Ψ_6 is 0, with the results reversed for the triangular lattice net 1. Where the calculation becomes more involved is in calculating Ψ for infinite periodic lattices having vertices of different valences or for finite platelets. For example, the unit cell of the historically important MacMahon net (net 18; see the Appendix) has vertices $\nu=3$ and $\nu=4$.

The pentagons comprising net 18 have two right angles, two angles of 114.295°, and one angle of 131.410°. Since the MacMahon pentagons are not in registry, either with a square-planar or triangular reference lattice, one expects (and finds) that the Ψ values will be different from "1" or "0," regardless of the choice of reference lattice. Moreover, when one considers a MacMahon platelet, some of the perimeter sites have valence, $\nu=2$. Accordingly, values of Ψ must be calculated for each of the N vertices of the net and the overall average constructed. The results reported in Table III are the average Ψ_4 and Ψ_6 values calculated for (almost) all the unit cells (of nets 1–27) specified in [6] and for the finite platelets displayed in the Appendix.

As a final point, in calculating Ψ, it is crucial to get the vertices and, especially, the angles "right," both for the unit cell and the companion platelet. The starting point (and acid test) here is to make sure that the packing fraction η for the unit cell is computed correctly. We have verified the packing fractions reported in [6] for all but one net, net 22; this is the only net for which we have not reported Ψ values [15].

IV. DISCUSSION

Presented in this study is an investigation of the proposal that finite chemical nets in the same O'Keeffe and Hyde compatibility class are characterized by very similar catalytic efficiencies. Evidence supporting this proposal was documented in Sec. II, viz., net 2 and net 6, net 2 and net 21, and the results presented in Table I. Moreover, differences in $\langle \bar{n} \rangle$ between or among companion platelets could be understood and ordered by comparing specific signatures of each finite lattice [1]: the total number N of lattice sites, the number N_b of boundary sites, the symmetry of the lattice [as quantified by the overall (average) root-mean-square distance of the N sites of the platelet relative to the centrosymmetric site], and the overall (average) valence (or connectivity) of the lattice. By way of comparison, in his study of $d=2$-dimensional random walks on infinite periodic lattices, Montroll proved

$$\langle n \rangle = \frac{N}{N-1}\{A_1 N \ln N + A_2 N + A_3 + A_4/N\}, \tag{2}$$

where the coefficients $\{A_1, A_2, A_3, A_4\}$ for hexagonal ($\nu=3$), square-planar ($\nu=4$), and triangular ($\nu=6$) lattices are given, respectively, by

$$\{A_1, A_2, A_3\} = \{3\sqrt{3}/4\pi, +0.066\ 206\ 698, -0.254\ 227\ 9\} \quad (\nu=3), \tag{3}$$

$$\{A_1, A_2, A_3, A_4\} = \{1/\pi, +0.195\ 056\ 166, -0.116\ 964\ 81, -0.051\ 456\ 50\} \quad (\nu=4), \tag{4}$$

$$\{A_1, A_2, A_3\} = \{\sqrt{3}/2\pi, +0.235\ 214\ 021, -0.251\ 407\ 596\} \quad (\nu=6). \tag{5}$$

As is seen from these expressions, for this class of lattices $\langle \bar{n} \rangle$ depends solely on N and (the uniform) valence ν.

In all cases studied here, the optimal locations for a catalytic site are in the interior of a finite platelet (see Tables

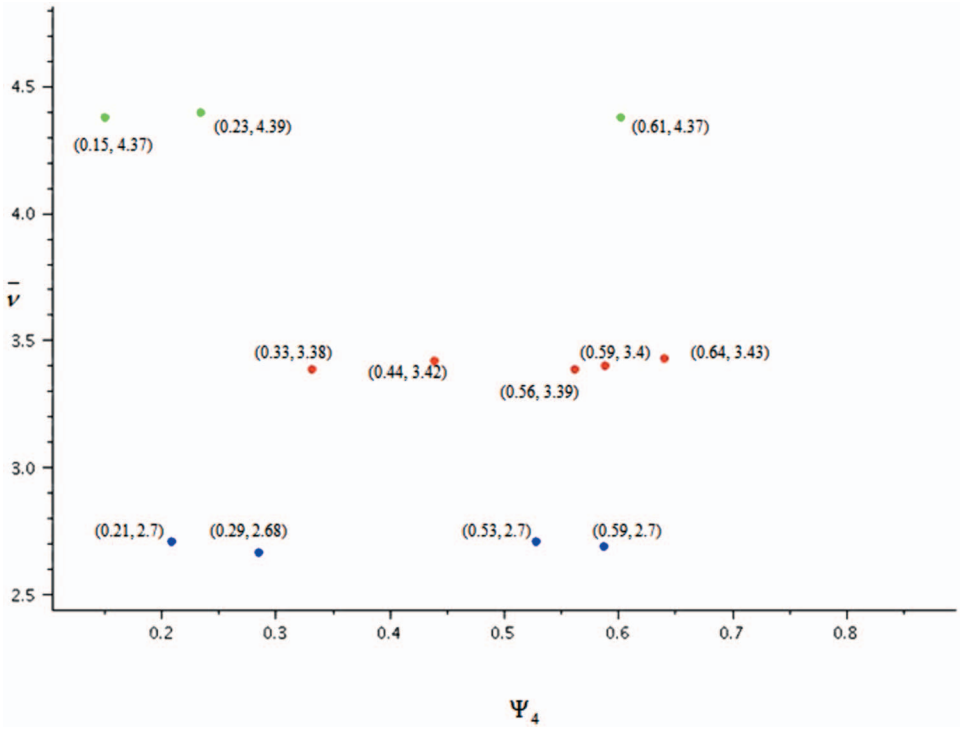

FIG. 5. (Color) Average valence $\bar{\nu}$ vs bond orientation function Ψ_4 for nets designated here by the couple $(\bar{\nu}, \Psi_4)$ (see text).

IV–VIIin the Appendix). While perhaps self-evident, this selectivity is more subtle for finite lattices than for infinite periodic ones; for the latter, the catalytic efficiency of all sites of a given valence at a given distance with respect to the reaction center (the "deep trap" site) would be exactly the same. This is not the case for platelets.

The advantage gained from the quantitative study presented here is that, in fabricating nanoplatelets, one can determine in the design phase which site locations in a specific geometry are likely to be optimal in facilitating the chemical transformation of a reactant; see the supplementary online material [13] accompanying this paper for a tabulation of the ratio R for (almost all) the platelets considered in this study. We reiterate that (almost all) the crystalline nets identified in the work of O'Keeffe and Hyde [6], and the ones studied here, have concrete realizations in known alloys and inorganic solids; thus, it may be hoped that the coded nets shown in the Appendix and the data tabulated in the supplementary online material [13] will be useful in analyzing results obtained in catalytic studies on "real" crystal surfaces [16].

An additional metric introduced in this study is the bond orientation function Ψ. Our interest in calculating Ψ for (almost all) the finite platelets derived from the 27 nets in [6] is that a precise characterization of the lattice geometry (both the angular relationship and the connectivity of adjacent vertices) must be specified in calculating Ψ. Thus, the pointwise symmetry of all sites N of the platelet relative to a square-planar or hexagonal reference lattice is captured in the calculation of Ψ. From the results displayed in Table III, several points emerge. First, the value of Ψ_4 (Ψ_6) calculated for finite arrays may be larger or smaller than value of Ψ_4 (Ψ_6) calculated for the unit cell of the parent net. Second, for platelets, there are instances where a net belonging to one of the O'Keeffe and Hyde compatibility classes (reference lattice), say the square-planar system, is characterized by a smaller Ψ value than Ψ calculated assuming the other (hexagonal) reference lattice, and vice versa. And, third, for three of the four nets identified in [6], which do not belong to either compatibility class, the values of Ψ_4 and Ψ_6 are remarkably similar.

Despite these "irregularities," a valuable insight can be drawn from the data in Tables II and III. For finite arrays, one finds that values of the overall $\bar{\nu}$ can cluster around specific values. Consider the nets characterized by values of $\bar{\nu}$ in the near vicinity of 2.7 (nets 9–11 and 26), of 3.4 (nets 8, 14*, 19, 24, and 25), and of 4.4 (nets 1, 4, 5, and 17). [Net 14* is a metrically square version of $\{3\cdot6\cdot3\cdot6, (3^2\cdot6^2)^2\}$, viz., the unit-cell parameters a and b of this tessellation are specified to be equal.] Taking the square-planar lattice as the reference lattice, a plot of Ψ_4 for nets in each of these clusters is presented in Fig. 5. These data demonstrate that, for finite arrays, a given setting of the (overall) lattice connectivity can correspond to platelets of quite different geometries and symmetries. In fact, there are instances (nets 8 and 19 in the second cluster and nets 4, 5, and 13 in the third) in which platelets belonging to *different* unit-cell compatibility classes are characterized by essentially the same catalytic activity, i.e., value of $\langle \bar{n} \rangle$.

Summarizing, in our study [5] of docking in postnucleation stages of self-assembly, it was proposed that the kinetics of platelet docking on protein crystallites or zeolite nanoparticles should be qualitatively similar for any geometry that results when a given structured surface is subjected to a diffeomorphic distortion (one that preserves values of N, N_b, and $\bar{\nu}$). To examine the validity of and to broaden this proposal, a corresponding states approach to chemical catalysis, the study presented here was undertaken. Transformations between or among members belonging to the same compatibility class, as identified in the seminal work of O'Keeffe and Hyde, were considered explicitly. By implementing the

theory of finite Markovian processes, numerically exact values of the mean walk length $\langle \bar{n} \rangle$ of a diffusing reactant before localization, a measure of the reaction efficiency, were calculated and the results obtained for nets belonging to the same compatibility class (see Tables I and II) were found to be remarkably similar. In fact, as noted in the preceding paragraph, examples were found wherein comparable catalytic activity was realized for platelets characterized by sensibly the same connectivity $[\bar{\nu}]$ but belonging to different compatibility classes.

In this study, we have focused on a "minimal" platelet for each of the geometries characterized by O'Keeffe and Hyde, viz., the planar nets displayed in their work [6]. The lattices diagrammed there are just large enough to encompass the unit cell for the arrangement of vertices and bonds defining a particular net. A further study could elaborate the program described here by considering larger and larger platelets; while more inclusive, one knows from earlier work in lattice statistics that differences in trapping efficiency between finite systems and infinite periodic lattices are most pronounced for small platelet sizes, with the behavior approaching that of infinite periodic lattices only gradually [3].

Our goal in this study was *not* to determine how large a platelet must be to approach asymptotically infinite system behavior, but rather to focus on the differences in catalytic activity that can arise when finite crystal nets are considered. Having that said, one knows that there are important problems in statistical mechanics for which the limitation to finite system size is not justified, e.g., phase transitions. In this context, note that if one were to replace "vertices" with "discs" and "bonds" with "contacts," the various geometrical characteristics defining planar crystalline nets (see Tables I–III) might be useful in describing structural aspects of the phase transition in a system of hard disks.

In a recent study [12], it was demonstrated computationally that topological transformations between and among crystalline planar nets, the program first introduced and described by O'Keeffe and Hyde over thirty years ago, can provide insight into the relationship between the symmetries of certain tessellations and the hard disk freezing transition. It was also noted that the percolated disk-disk contacts described by the tessellation, net 21 (see Figs. 1 and 2), were characterized (overall) by a packing fraction (η=0.677) *smaller* than the packing fractions of the tessellations $[3\cdot6\cdot4\cdot6]$ and $[3\cdot6\cdot3\cdot6]$ (η=0.729 and η=0.680, respectively) that believed to bracket the KTHNY hexatic phase (which lies between the melting and the freezing transition). Taken together, these observations led to a renormalization strategy which tracked the (possible) structural changes in a system of hard disks from the fluid to hexatic to solid phase. The analytical and the computational results obtained were found to be consistent with the most extensive Monte Carlo evidence on the hard disk phase transition reported by Mak [17].

ACKNOWLEDGMENTS

The authors would like to acknowledge D. Low, U. Gomez, R. Swaroop, C. Ramirez, and B. Coreas for generating and verifying some of the data for this paper. This work was supported by grants from the Howard Hughes Medical Institute and the Summer Undergraduate Research Program granted to Pomona College.

APPENDIX

Figures 6–39 exhibit the planar nets considered in this work (redrawn from [6]) (see Tables IV–VII).

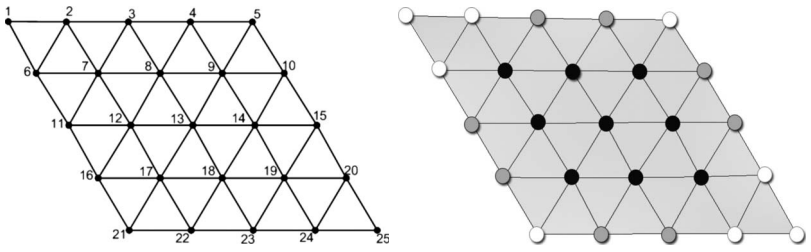

FIG. 6. Net 1.

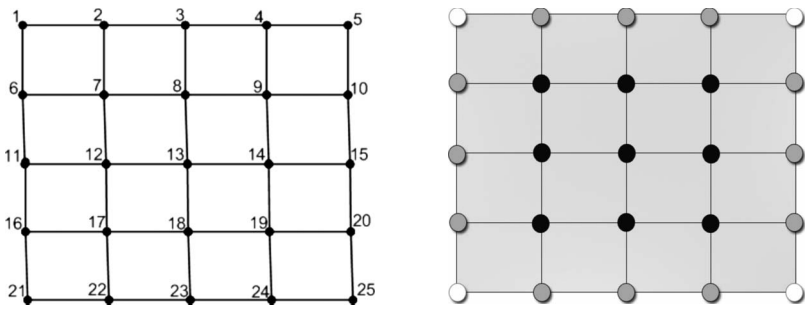

FIG. 7. Net 2.

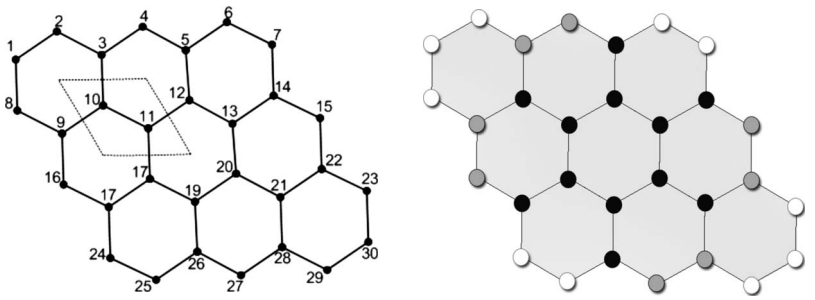

FIG. 8. Net. 3.

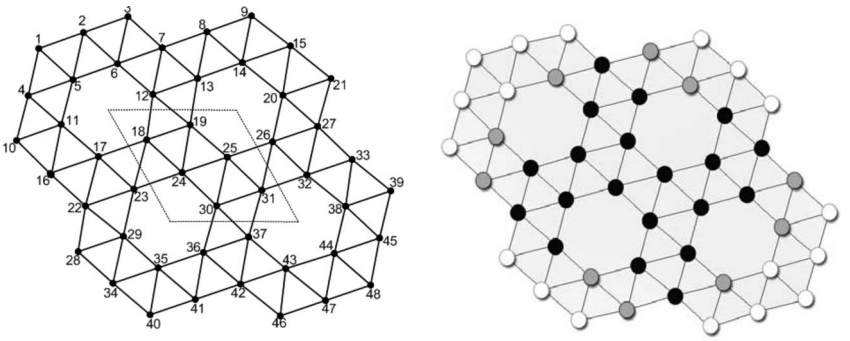

FIG. 9. Net 4a.

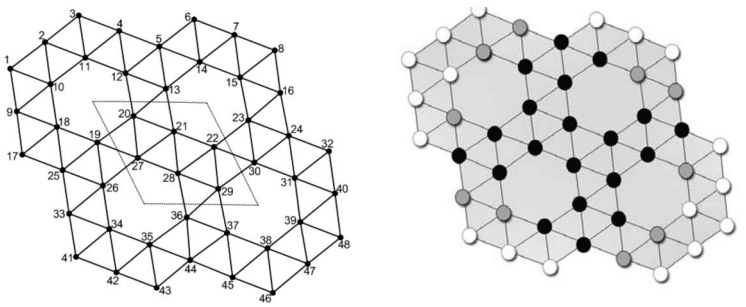

FIG. 10. Net 4b.

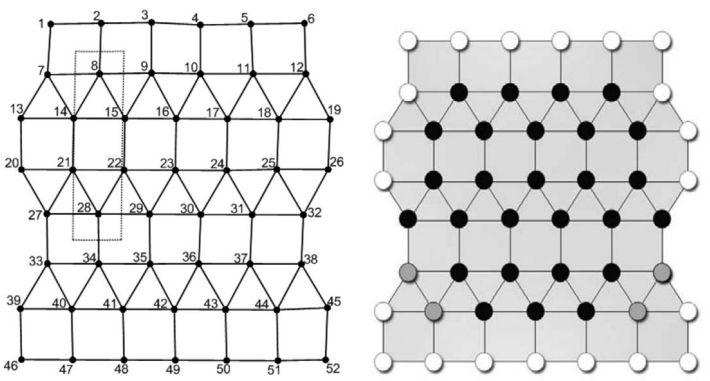

FIG. 11. Net 5.

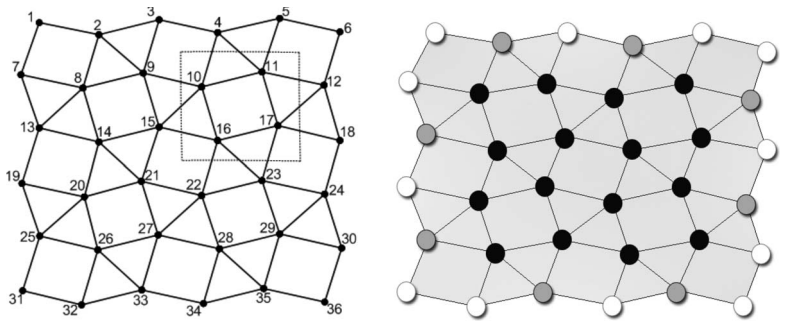

FIG. 12. Net 6.

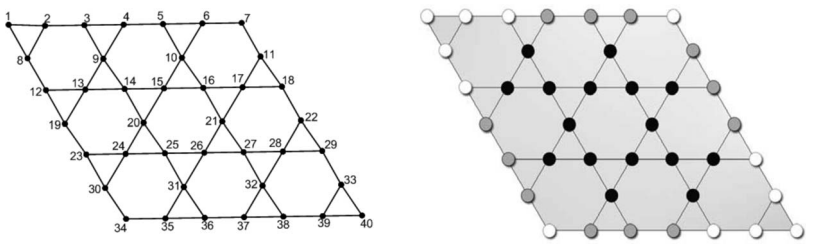

FIG. 13. Net 7.

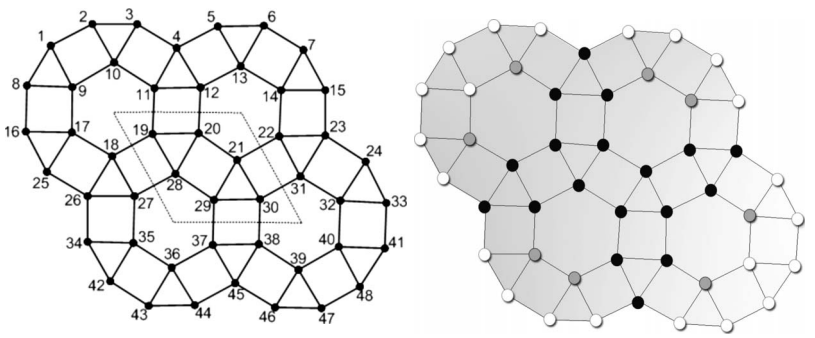

FIG. 14. Net 8.

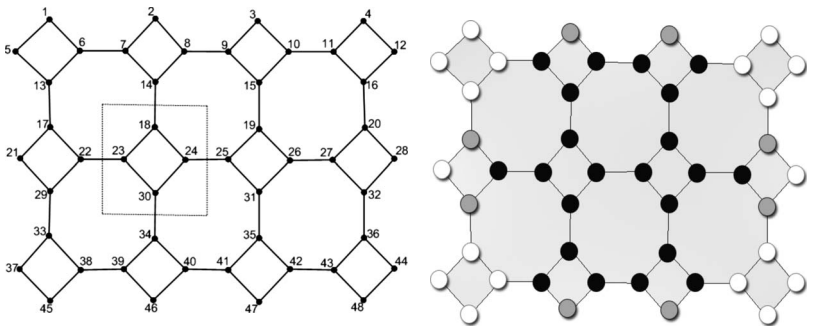

FIG. 15. Net 9.

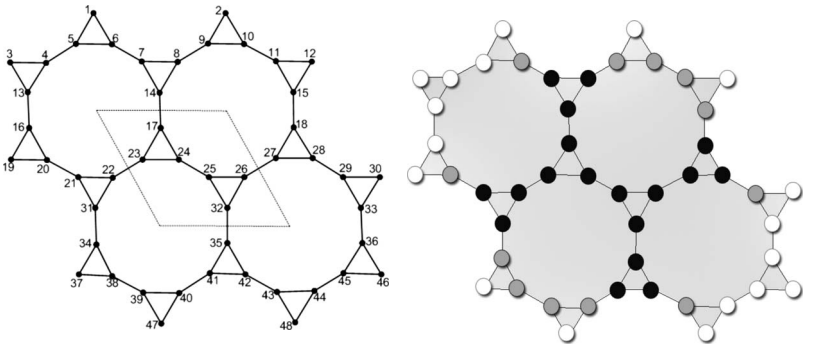

FIG. 16. Net 10.

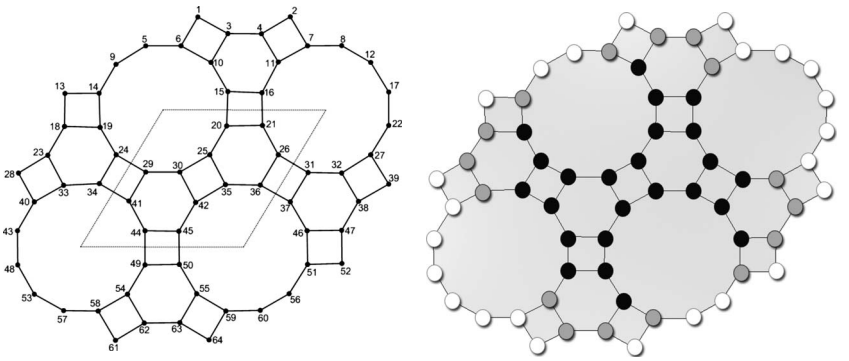

FIG. 17. Net 11.

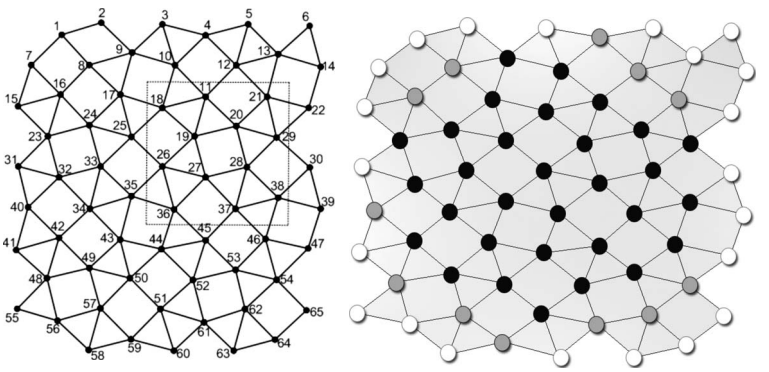

FIG. 18. Net 12.

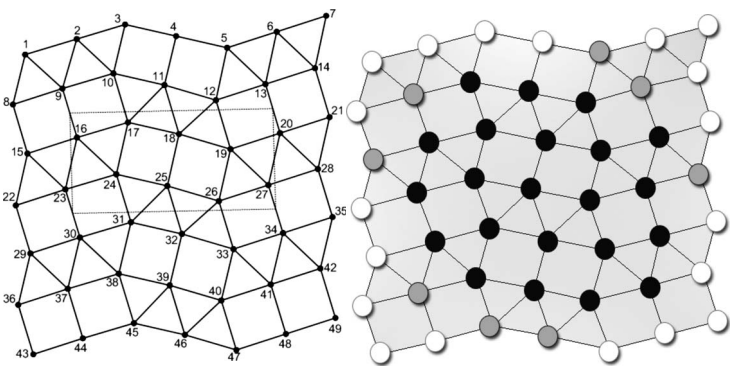

FIG. 19. Net 13.1.

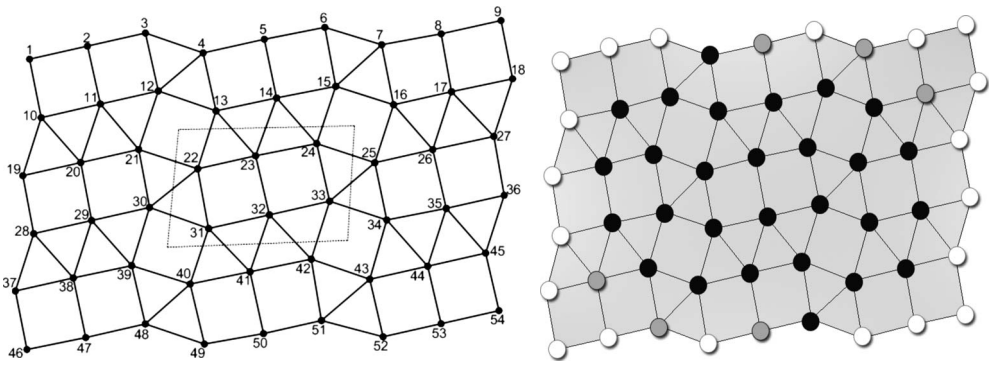

FIG. 20. Net 13a.

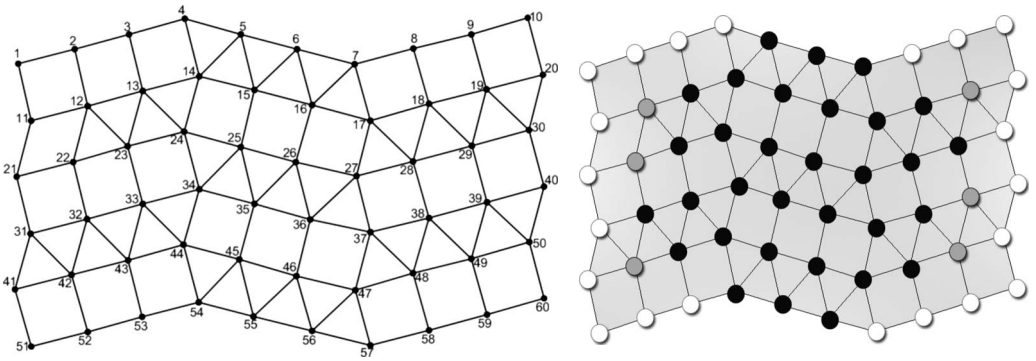

FIG. 21. Net 13b.

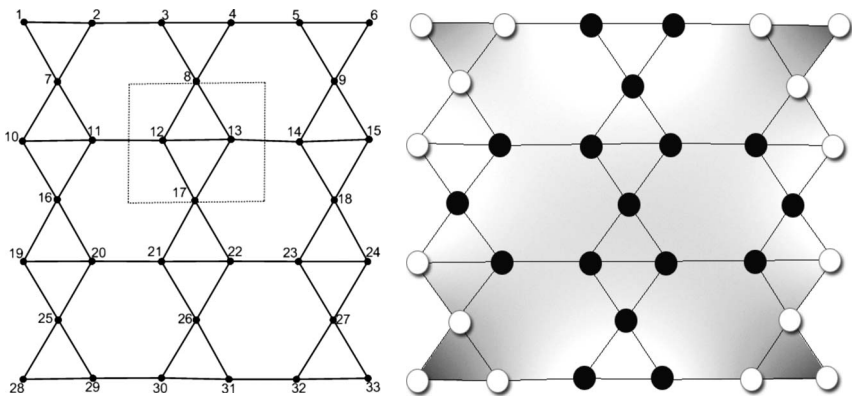

FIG. 22. Net 14.

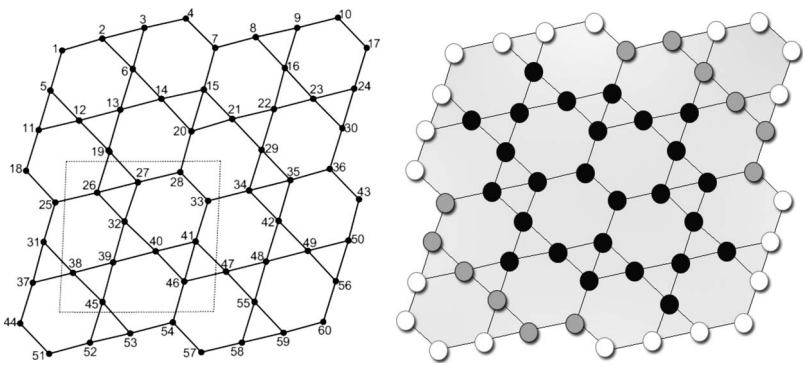

FIG. 23. Net 15.

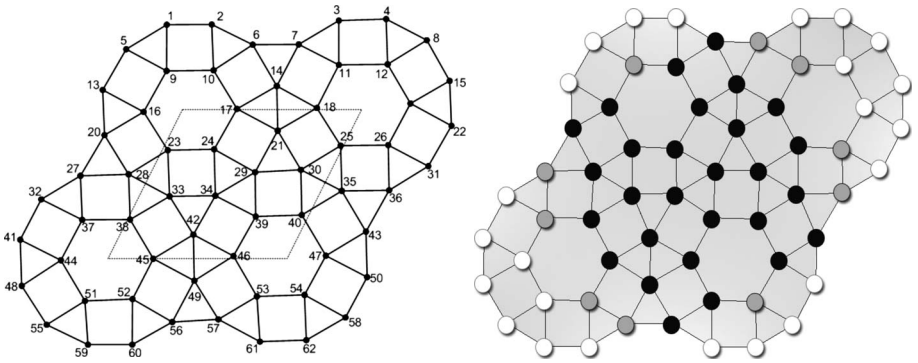

FIG. 24. Net 16a.

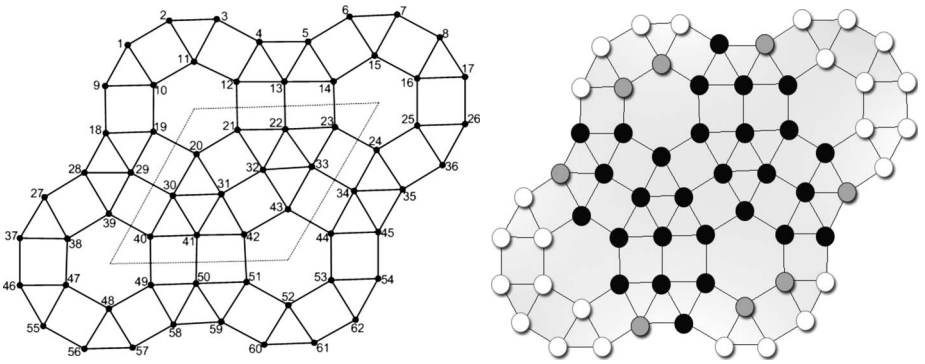

FIG. 25. Net 16b.

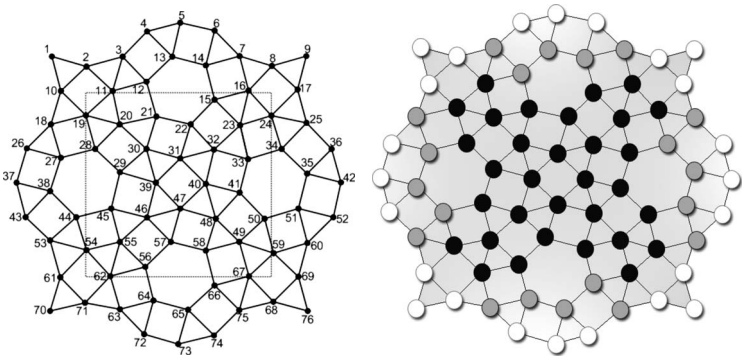

FIG. 26. Net 17a.

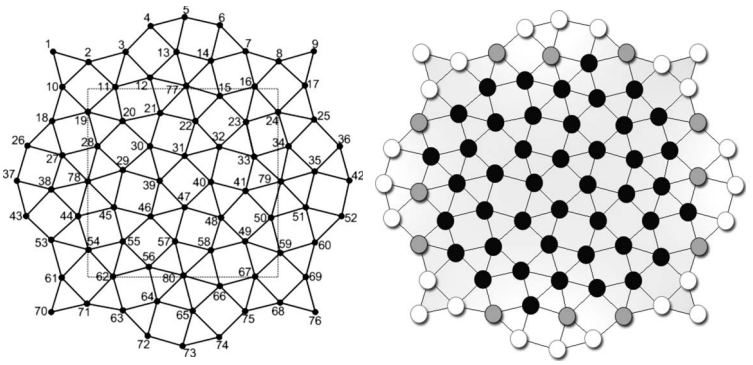

FIG. 27. Net 17b.

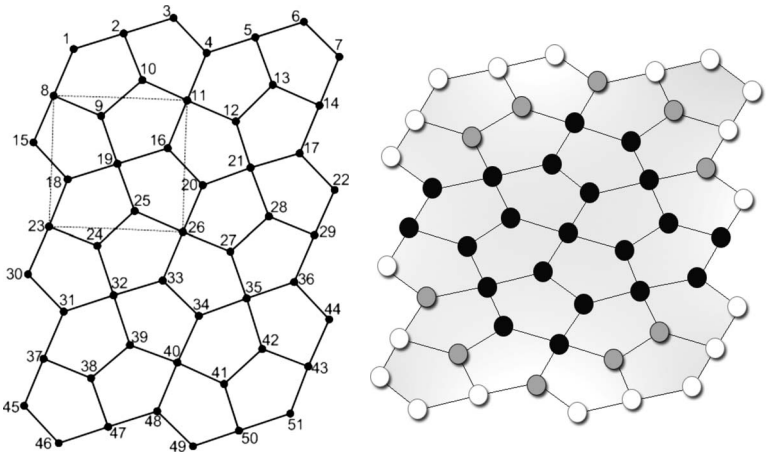

FIG. 28. Net 18.

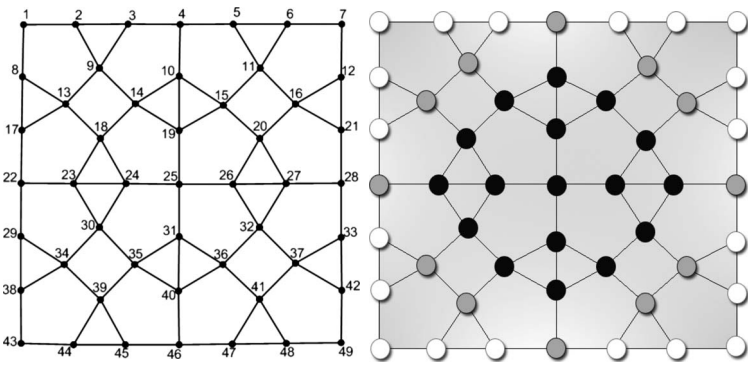

FIG. 29. Net 19.

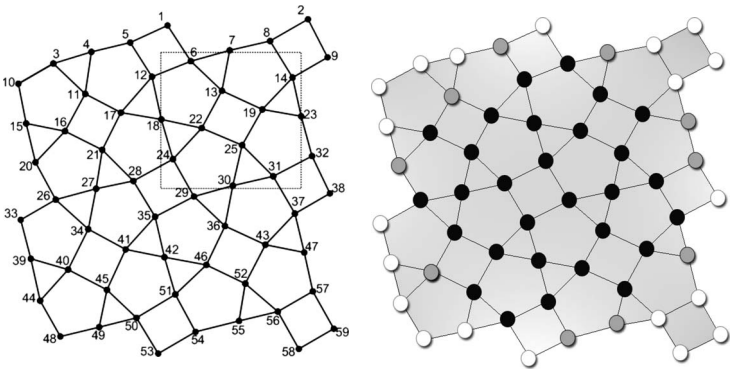

FIG. 30. Net 20a.

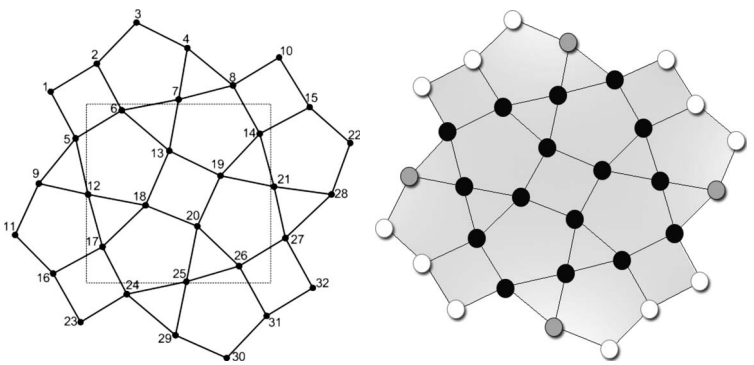

FIG. 31. Net 20b.

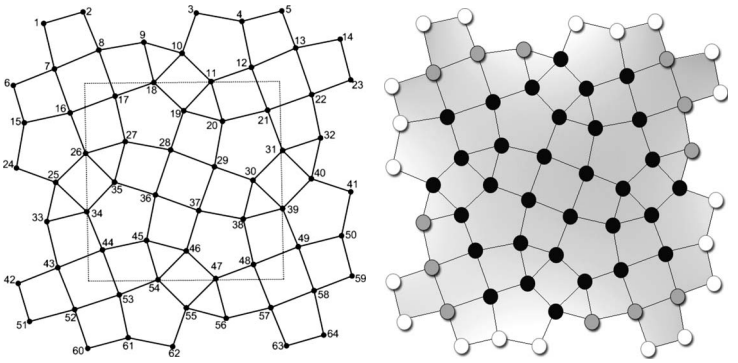

FIG. 32. Net 21a.

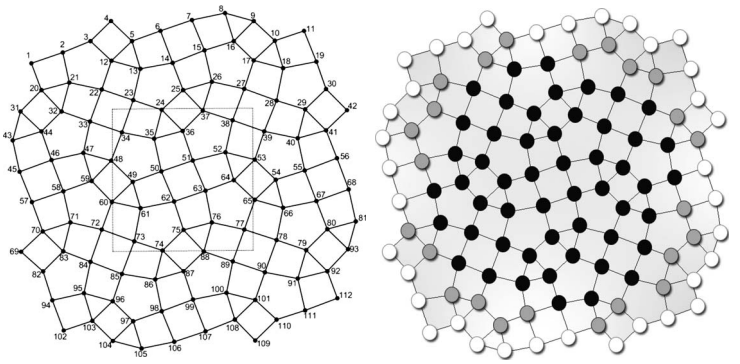

FIG. 33. Net 21b.

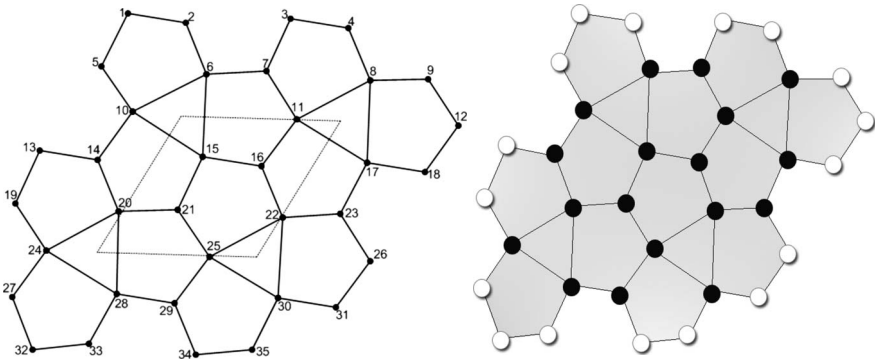

FIG. 34. Net 22.

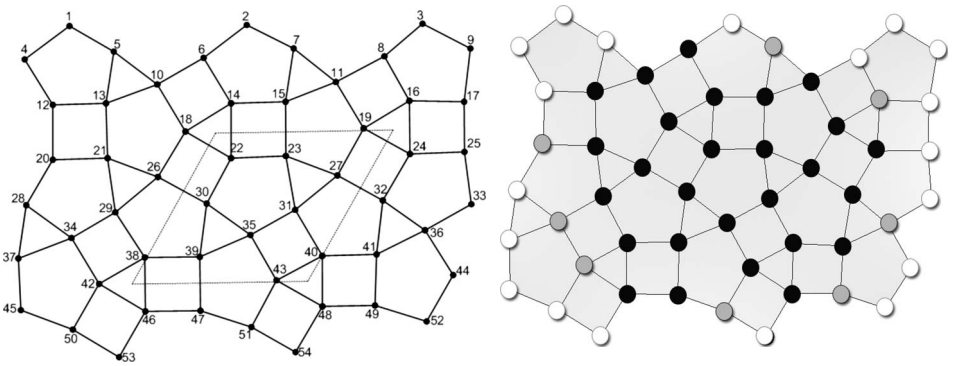

FIG. 35. Net 23.

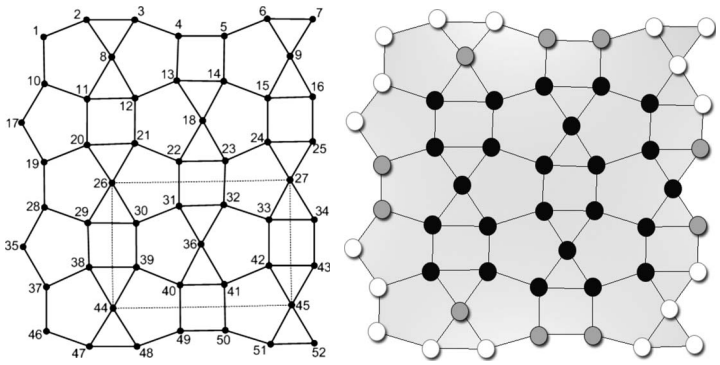

FIG. 36. Net 24.

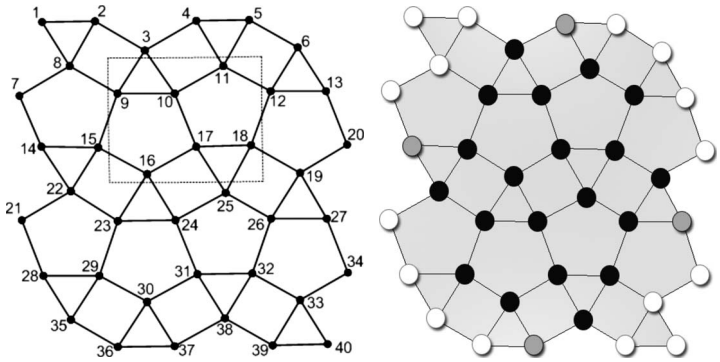

FIG. 37. Net 25.

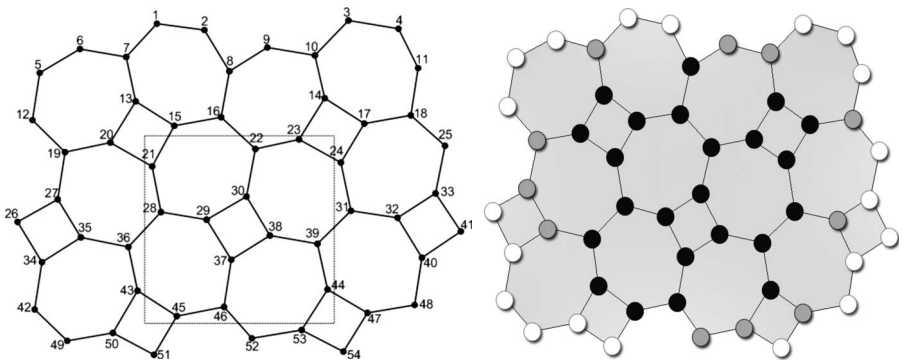

FIG. 38. Net 26.

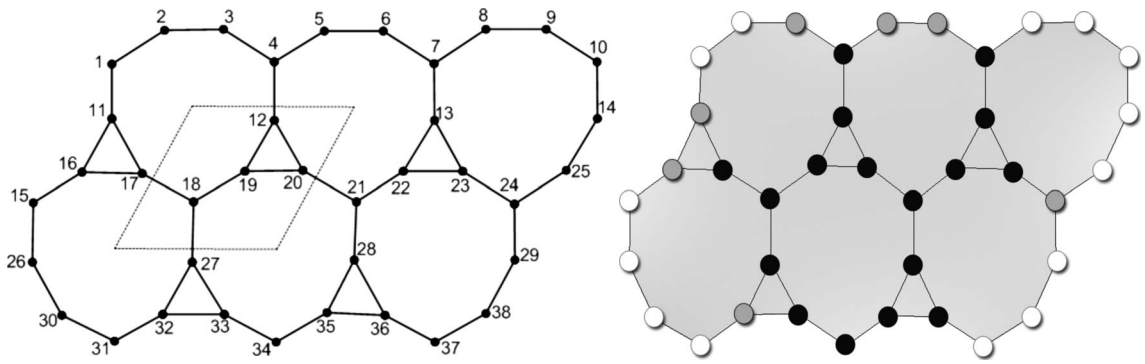

FIG. 39. Net 27.

TABLE IV. Ratios $\langle n(i)\rangle/\langle n(\text{ave})\rangle$ vs trap sites for nets 1–3, 4a, 4b, and 5–8. The $\langle n(\text{ave})\rangle$ value for each of the nets below is given in Table I.

T	Net 1 (N=25)	Net 2 (N=25)	Net 3 (N=30)	Net 4a (N=48)	Net 4b (N=48)	Net 5 (N=52)	Net 6 (N=36)	Net 7 (N=40)	Net 8 (N=48)
1	2.239	1.593	1.615	1.540	1.540	1.822	1.836	2.051	1.410
2	1.287	1.096	1.447	1.262	1.313	1.357	1.038	1.580	1.329
3	0.960	0.971	0.942	1.335	1.452	1.210	1.129	1.145	1.194
4	0.913	1.096	1.062	1.313	1.070	1.210	0.936	1.001	0.845
5	1.208	1.593	0.801	1.115	0.826	1.357	1.352	0.929	1.112
6	1.287	1.096	1.163	0.953	1.251	1.822	1.836	0.988	1.193
7	0.745	0.728	1.163	0.843	1.114	1.114	1.352	1.293	1.193
8	0.570	0.631	1.447	1.001	1.320	0.842	0.805	1.580	1.410
9	0.600	0.728	0.942	1.320	1.262	0.738	0.718	0.824	1.126
10	0.913	1.096	0.756	1.452	1.115	0.738	0.630	0.690	1.015
11	0.960	0.971	0.592	1.040	1.040	0.842	0.805	0.988	0.760
12	0.570	0.631	0.604	0.712	0.787	1.114	1.038	1.145	0.732
13	0.485	0.544	0.604	0.751	0.694	1.227	0.936	0.824	0.901
14	0.570	0.631	0.801	0.906	0.861	0.816	0.630	0.635	0.901
15	0.960	0.971	1.062	1.114	0.906	0.672	0.556	0.566	1.112
16	0.913	1.096	1.062	1.070	1.001	0.628	0.556	0.574	1.329
17	0.600	0.728	0.801	0.787	1.335	0.672	0.718	0.690	1.015
18	0.570	0.631	0.604	0.641	0.953	0.816	1.129	0.929	0.760
19	0.745	0.728	0.604	0.619	0.712	1.227	1.129	1.001	0.653
20	1.287	1.096	0.592	0.861	0.641	1.139	0.718	0.566	0.619
21	1.208	1.593	0.756	1.251	0.595	0.712	0.556	0.566	0.619
22	0.913	1.096	0.942	0.826	0.619	0.578	0.556	1.001	0.732
23	0.960	0.971	1.447	0.694	0.751	0.540	0.630	0.929	0.845
24	1.287	1.096	1.163	0.595	0.843	0.578	0.936	0.690	1.194
25	2.239	1.593	1.163	0.595	0.843	0.712	1.038	0.574	1.194
26			0.801	0.694	0.751	1.139	0.805	0.566	0.845
27			1.062	0.826	0.619	0.856	0.630	0.635	0.732
28			0.942	1.251	0.595	0.625	0.718	0.824	0.619
29			1.447	0.861	0.641	0.546	0.805	1.145	0.619
30			1.615	0.619	0.712	0.546	1.352	0.988	0.653
31				0.641	0.953	0.625	1.836	0.690	0.760
32				0.787	1.335	0.856	1.352	0.824	1.015
33				1.070	1.001	0.977	0.936	1.580	1.329
34				1.114	0.906	0.722	1.129	1.293	1.112
35				0.906	0.861	0.629	1.038	0.988	0.901
36				0.751	0.694	0.629	1.836	0.929	0.901
37				0.712	0.787	0.722		1.001	0.732
38				1.040	1.040	0.977		1.145	0.760
39				1.452	1.115	1.459		1.580	1.015
40				1.320	1.262	0.944		2.051	1.126
41				1.001	1.320	0.765			1.410
42				0.843	1.114	0.713			1.193
43				0.953	1.251	0.765			1.193
44				1.115	0.826	0.944			1.112
45				1.313	1.070	1.459			0.845
46				1.335	1.452	2.027			1.194
47				1.262	1.313	1.458			1.329
48				1.540	1.540	1.237			1.410
49						1.175			
50						1.237			
51						1.458			
52						2.027			

TABLE V. Ratios $\langle n(i)\rangle/\langle n(\text{ave})\rangle$ vs trap sites for nets 9–12, 13.1, 13a, 13b, 14, and 15. The $\langle n(\text{ave})\rangle$ value for each of the nets below is given in Table I.

T	Net 9 (N=48)	Net 10 (N=48)	Net 11 (N=64)	Net 12 (N=65)	Net 13.1 (N=49)	Net 13a (N=54)	Net 13b (N=60)	Net 14 (N=33)	Net 15 (N=60)
1	1.554	1.362	1.209	1.467	1.448	1.845	1.963	1.775	1.465
2	1.070	1.234	1.292	1.389	1.159	1.378	1.419	1.322	1.175
3	1.070	1.508	0.986	1.215	1.261	1.203	1.221	0.505	1.143
4	1.554	1.266	1.022	1.078	1.128	0.877	1.149	0.505	1.340
5	1.562	1.178	1.173	1.367	0.987	1.014	0.888	1.322	1.175
6	1.101	1.062	0.997	2.150	1.292	1.108	0.814	1.775	0.858
7	0.882	0.799	1.130	1.462	2.052	0.969	0.811	1.101	0.960
8	0.781	0.775	1.443	0.967	1.343	1.410	1.154	0.786	1.099
9	0.781	0.961	1.173	0.882	0.975	2.033	1.480	1.101	1.287
10	0.882	1.023	0.876	0.817	0.844	1.151	2.062	1.104	1.802
11	1.101	1.023	0.936	0.698	0.693	0.873	1.449	0.827	1.143
12	1.562	1.234	1.600	0.947	0.688	0.764	0.919	0.643	0.858
13	1.124	1.266	1.209	1.195	0.900	0.622	0.773	0.643	0.720
14	0.723	0.700	0.997	1.697	1.289	0.622	0.742	0.827	0.681
15	0.723	0.961	0.728	1.377	0.967	0.720	0.666	1.104	0.674
16	1.124	1.178	0.749	0.960	0.715	0.766	0.633	0.858	0.945
17	0.966	0.602	1.600	0.727	0.640	1.000	0.648	0.603	1.802
18	0.615	0.775	0.986	0.659	0.592	1.528	0.803	0.858	1.340
19	0.615	1.362	0.876	0.610	0.617	1.261	1.049	1.104	0.681
20	0.966	1.062	0.631	0.699	0.778	0.867	1.563	0.827	0.619
21	1.204	0.799	0.657	0.910	1.226	0.698	1.303	0.643	0.630
22	0.820	0.700	1.443	1.343	1.151	0.578	0.972	0.643	0.733
23	0.649	0.602	1.022	0.860	0.742	0.552	0.744	0.827	0.945
24	0.568	0.569	0.728	0.718	0.603	0.583	0.639	1.104	1.287
25	0.568	0.569	0.569	0.623	0.549	0.641	0.558	1.101	0.960
26	0.649	0.602	0.657	0.561	0.576	0.811	0.544	0.786	0.674
27	0.820	0.700	1.130	0.584	0.677	1.122	0.578	1.101	0.619
28	1.204	0.799	1.292	0.665	0.948	1.122	0.680	1.775	0.660
29	0.966	1.062	0.631	0.807	1.050	0.811	0.857	1.322	0.630
30	0.615	1.362	0.569	1.180	0.735	0.641	1.163	0.505	1.099
31	0.615	0.775	0.749	1.171	0.593	0.583	1.170	0.505	1.099
32	0.966	0.602	0.936	0.776	0.580	0.552	0.869	1.322	0.630
33	1.124	1.178	0.936	0.635	0.670	0.578	0.687	1.775	0.660
34	0.723	0.961	0.749	0.651	0.801	0.698	0.581		0.619
35	0.723	0.700	0.569	0.584	1.184	0.867	0.544		0.674
36	1.124	1.266	0.631	0.569	1.493	1.261	0.557		0.960
37	1.562	1.234	0.728	0.653	0.940	1.528	0.636		1.287
38	1.101	1.023	1.022	0.810	0.719	1.000	0.737		0.945
39	0.882	1.023	1.292	1.273	0.728	0.766	0.905		0.733
40	0.781	0.961	1.130	1.004	0.805	0.720	1.288		0.630
41	0.781	0.775	0.657	1.249	0.851	0.622	1.569		0.619

TABLE V. (*Continued.*)

T	Net 9 (N=48)	Net 10 (N=48)	Net 11 (N=64)	Net 12 (N=65)	Net 13.1 (N=49)	Net 13a (N=54)	Net 13b (N=60)	Net 14 (N=33)	Net 15 (N=60)
42	0.882	0.799	0.569	0.843	1.113	0.622	1.057		0.681
43	1.101	1.062	1.443	0.639	2.038	0.764	0.810		1.340
44	1.562	1.178	0.657	0.623	1.385	0.873	0.652		1.802
45	1.554	1.266	0.631	0.627	0.938	1.151	0.634		0.945
46	1.070	1.508	0.876	0.802	0.979	2.033	0.665		0.674
47	1.070	1.234	0.986	1.230	1.273	1.410	0.739		0.681
48	1.554	1.362	1.600	1.000	1.408	0.969	0.767		0.720
49			0.749	0.778	1.877	1.108	0.904		0.858
50			0.728	0.715		1.014	1.178		1.143
51			0.997	0.840		0.877	2.069		1.802
52			1.209	0.712		1.203	1.486		1.287
53			1.600	0.769		1.378	1.159		1.099
54			0.936	0.946		1.845	0.814		0.960
55			0.876	1.839			0.815		0.858
56			1.173	1.229			0.887		1.175
57			1.443	0.933			1.144		1.340
58			1.130	1.364			1.210		1.143
59			0.997	1.087			1.384		1.175
60			1.173	1.244			1.840		1.465
61			1.292	0.902					
62			1.022	1.005					
63			0.986	1.428					
64			1.209	1.585					
65				1.873					

TABLE VI. Ratios $\langle n(\mathrm{i})\rangle/\langle n(\mathrm{ave})\rangle$ vs trap sites for nets 16a, 16b, 17a, 17b, 18, 19, 20a, 20b, and 21a. The $\langle n(\mathrm{ave})\rangle$ value for each of the nets below is given in Table I.

T	Net 16a (N=62)	Net 16b (N=62)	Net 17a (N=76)	Net 17b (N=80)	Net 18 (N=51)	Net 19 (N=49)	Net 20a (N=59)	Net 20b (N=32)	Net 21a (N=64)
1	1.296	1.287	1.792	1.992	1.437	1.676	1.366	1.436	1.748
2	1.166	1.287	1.159	1.248	1.174	1.291	1.989	1.165	1.705
3	1.280	1.190	1.033	1.077	1.381	1.141	1.261	1.513	1.349
4	1.498	0.868	1.333	1.380	1.024	0.990	1.148	1.061	1.203
5	1.296	0.906	1.396	1.442	1.169	1.141	1.076	0.804	1.531
6	0.881	1.316	1.311	1.363	1.675	1.291	0.845	0.716	1.531
7	0.923	1.475	1.048	1.088	1.661	1.676	1.052	0.731	1.070
8	1.569	1.570	1.151	1.241	1.130	1.291	1.350	0.804	0.941
9	1.013	1.190	1.792	1.992	0.912	0.910	1.908	1.061	0.943
10	0.883	0.981	1.151	1.241	0.944	0.732	1.591	1.436	0.801
11	0.988	0.981	0.849	0.878	0.705	0.910	0.901	1.513	0.688
12	1.242	0.770	0.910	0.819	0.813	1.291	0.744	0.731	0.825
13	1.166	0.704	1.091	0.953	1.041	0.910	0.760	0.575	1.070
14	0.679	0.836	1.015	0.897	1.127	0.691	1.109	0.716	1.748
15	1.569	1.144	0.814	0.748	1.281	0.691	1.212	1.165	1.203
16	0.883	1.275	0.830	0.863	0.699	0.910	0.865	1.165	0.825
17	0.690	1.570	1.159	1.248	0.913	1.141	0.680	0.716	0.710
18	0.746	0.868	1.048	1.088	0.865	0.691	0.638	0.575	0.725
19	1.242	0.770	0.830	0.863	0.619	0.653	0.808	0.575	0.619
20	0.881	0.628	0.701	0.726	0.647	0.691	1.034	0.575	0.616
21	0.581	0.628	0.731	0.690	0.613	1.141	0.644	0.731	0.710
22	1.498	0.572	0.690	0.663	1.174	0.990	0.604	1.513	0.941
23	0.690	0.703	0.701	0.726	0.861	0.732	1.050	1.436	1.705
24	0.616	0.836	0.849	0.878	0.731	0.653	0.553	0.804	1.349
25	0.746	1.144	1.033	1.077	0.654	0.535	0.632	0.731	0.801
26	0.988	1.475	1.311	1.363	0.499	0.653	0.781	0.716	0.688
27	0.923	1.316	1.015	0.897	0.654	0.732	0.661	0.804	0.616
28	0.679	0.906	0.814	0.748	0.731	0.990	0.567	1.061	0.527
29	0.523	0.704	0.690	0.663	0.861	1.141	0.545	1.061	0.527
30	0.581	0.572	0.591	0.631	1.174	0.691	0.613	1.513	0.619
31	1.280	0.532	0.556	0.606	0.913	0.653	0.705	1.165	0.725
32	1.280	0.532	0.591	0.631	0.613	0.691	1.018	1.436	0.943
33	0.581	0.572	0.731	0.690	0.647	1.141	1.373		0.943
34	0.523	0.704	0.910	0.819	0.699	0.910	0.694		0.725
35	0.679	0.906	1.091	0.953	0.619	0.691	0.559		0.619
36	0.923	1.316	1.333	1.380	0.865	0.691	0.596		0.527
37	0.988	1.475	1.396	1.442	1.127	0.910	0.819		0.527
38	0.746	1.144	1.091	0.953	1.041	1.291	1.325		0.616
39	0.616	0.836	0.556	0.606	0.813	0.910	1.240		0.688
40	0.690	0.703	0.556	0.606	0.705	0.732	0.917		0.801
41	1.498	0.572	0.690	0.663	0.944	0.910	0.634		1.349

TABLE VI. (*Continued.*)

T	Net 16a (N=62)	Net 16b (N=62)	Net 17a (N=76)	Net 17b (N=80)	Net 18 (N=51)	Net 19 (N=49)	Net 20a (N=59)	Net 20b (N=32)	Net 21a (N=64)
42	0.581	0.628	1.396	1.442	0.912	1.291	0.636		1.705
43	0.881	0.628	1.333	1.380	1.130	1.676	0.749		0.941
44	1.242	0.770	0.910	0.819	1.281	1.291	1.286		0.710
45	0.746	0.868	0.731	0.690	1.661	1.141	0.818		0.616
46	0.690	1.570	0.591	0.631	1.675	0.990	0.644		0.619
47	0.883	1.275	0.556	0.606	1.169	1.141	1.038		0.725
48	1.569	1.144	0.591	0.631	1.024	1.291	1.568		0.710
49	0.679	0.836	0.701	0.726	1.381	1.676	1.140		0.825
50	1.166	0.704	0.814	0.748	1.174		0.878		1.203
51	1.242	0.770	1.015	0.897	1.437		0.735		1.748
52	0.988	0.981	1.311	1.363			0.812		1.070
53	0.883	0.981	1.033	1.077			1.368		0.825
54	1.013	1.190	0.849	0.878			1.046		0.688
55	1.569	1.570	0.701	0.726			1.061		0.801
56	0.923	1.475	0.814	0.748			1.112		0.943
57	0.881	1.316	0.690	0.663			1.346		0.941
58	1.296	0.906	0.731	0.690			1.909		1.070
59	1.498	0.868	0.830	0.863			1.987		1.531
60	1.280	1.190	1.048	1.088					1.531
61	1.166	1.287	1.159	1.248					1.203
62	1.296	1.287	0.830	0.863					1.349
63			1.048	1.09					1.705
64			1.015	0.897					1.748
65			1.091	0.953					
66			0.910	0.819					
67			0.849	0.878					
68			1.159	1.248					
69			1.151	1.241					
70			1.792	1.992					
71			1.151	1.241					
72			1.311	1.363					
73			1.396	1.442					
74			1.333	1.380					
75			1.033	1.077					
76			1.792	1.992					
77				0.698					
78				0.698					
79				0.698					
80				0.698					

TABLE VII. Ratios $\langle n(i)\rangle/\langle n(\text{ave})\rangle$ vs trap sites for nets 21b, 22–27, and 39a (right and left). The $\langle n(\text{ave})\rangle$ value for each of the nets below is given in Table I.

T	Net 21b (N=112)	Net 22 (N=35)	Net 23 (N=54)	Net 24 (N=52)	Net 25 (N=40)	Net 26 (N=54)	Net 27 (N=38)	Net 39 a right (N=88)	Net 39 a left (N=88)
1	1.703	1.521	1.799	1.649	1.779	1.262	1.191	1.567	1.589
2	1.363	1.288	1.269	1.299	1.330	1.195	1.222	1.812	1.830
3	1.326	1.278	1.802	1.155	0.851	1.395	1.064	1.355	1.424
4	1.623	1.303	1.809	0.998	1.095	1.560	0.717	1.289	1.289
5	1.046	1.288	1.179	1.057	1.173	1.547	0.957	0.873	1.143
6	1.108	0.590	0.892	1.385	1.185	1.429	0.999	1.590	1.224
7	1.187	0.752	0.944	1.807	1.451	1.027	0.843	1.872	1.820
8	1.329	0.825	1.145	0.952	1.126	0.828	1.282	1.872	1.820
9	1.332	1.494	1.852	1.179	0.762	1.046	1.550	1.099	1.111
10	1.169	0.590	0.770	1.256	0.697	0.944	1.649	0.872	0.905
11	1.703	0.597	0.756	0.832	0.883	1.440	0.971	0.958	0.828
12	0.987	1.699	1.208	0.725	0.865	1.379	0.614	0.942	0.909
13	0.887	1.278	0.882	0.715	1.185	0.815	0.746	1.277	1.082
14	0.855	0.752	0.632	0.754	1.022	0.802	1.577	1.812	1.830
15	0.914	0.466	0.655	0.876	0.694	0.697	1.348	1.277	1.082
16	1.093	0.550	0.941	1.141	0.580	0.634	1.009	0.764	0.832
17	1.002	0.715	1.294	1.507	0.567	0.837	0.849	0.704	0.720
18	1.055	1.439	0.608	0.649	0.628	1.035	0.617	0.703	0.725
19	1.363	1.303	0.752	1.040	0.766	0.925	0.589	0.741	0.831
20	1.169	0.597	1.036	0.717	1.359	0.792	0.565	1.099	1.111
21	1.055	0.550	0.738	0.622	1.359	0.688	0.519	0.942	1.224
22	0.845	0.507	0.559	0.569	0.766	0.575	0.664	0.741	0.831
23	0.746	0.742	0.555	0.598	0.628	0.687	0.765	0.631	0.678
24	0.709	0.825	0.848	0.758	0.567	0.734	0.924	0.626	0.633
25	0.763	0.507	1.175	1.025	0.580	1.236	1.335	0.652	0.680
26	0.789	1.216	0.605	0.656	0.694	1.334	1.508	0.764	0.832
27	0.792	1.494	0.608	0.815	1.022	1.000	0.768	1.355	1.424
28	0.845	0.715	1.145	1.040	1.185	0.615	0.679	1.590	1.589
29	0.987	0.742	0.698	0.717	0.865	0.603	1.177	0.873	0.909
30	1.326	0.651	0.544	0.622	0.883	0.591	1.489	0.652	0.680
31	1.332	1.185	0.560	0.569	0.697	0.722	1.290	0.578	0.594
32	1.002	1.699	0.738	0.598	0.762	0.958	0.911	0.583	0.595
33	0.792	1.439	1.408	0.758	1.126	1.114	0.816	0.631	0.678
34	0.698	1.216	0.923	1.025	1.451	1.163	0.888	0.872	0.905
35	0.669	1.185	0.555	1.507	1.185	0.946	0.751	1.567	1.143
36	0.676		0.938	0.649	1.173	0.748	0.804	0.703	0.725
37	0.727		1.276	1.256	1.095	0.640	1.117	0.583	0.595
38	0.698		0.733	0.832	0.851	0.622	1.241	0.513	0.556
39	0.746		0.608	0.725	1.330	0.675		0.578	0.594
40	0.887		0.677	0.715	1.779	1.117		0.704	0.720
41	1.046		0.784	0.754		1.368		1.289	1.289
42	1.623		0.902	0.876		1.448		0.958	0.828
43	1.329		0.696	1.141		0.896		0.626	0.633
44	1.093		1.604	0.952		0.885		0.513	0.556
45	1.187		1.635	1.179		0.895		0.513	0.556
46	0.914		0.874	1.649		0.734		0.626	0.633

TABLE VII. (*Continued.*)

T	Net 21b (N=112)	Net 22 (N=35)	Net 23 (N=54)	Net 24 (N=52)	Net 25 (N=40)	Net 26 (N=54)	Net 27 (N=38)	Net 39 a right (N=88)	Net 39 a left (N=88)
47	0.789		0.832	1.299		1.064		0.958	0.828
48	0.727		0.812	1.155		1.249		1.288	1.289
49	0.676		1.064	0.998		1.432		0.704	0.720
50	0.610		1.313	1.057		1.117		0.578	0.594
51	0.610		0.937	1.385		1.258		0.513	0.556
52	0.669		1.646	1.807		1.027		0.583	0.595
53	0.709		1.500			0.992		0.703	0.725
54	0.763		1.287			1.280		1.567	1.143
55	0.855							0.872	0.905
56	1.108							0.631	0.678
57	1.108							0.583	0.595
58	0.855							0.578	0.594
59	0.763							0.652	0.680
60	0.709							0.873	0.909
61	0.669							1.590	1.589
62	0.610							1.355	1.424
63	0.610							0.764	0.832
64	0.676							0.652	0.680
65	0.727							0.626	0.633
66	0.789							0.631	0.678
67	0.914							0.741	0.831
68	1.187							0.942	1.224
69	1.623							1.099	1.111
70	1.046							0.741	0.831
71	0.887							0.703	0.725
72	0.746							0.704	0.720
73	0.698							0.764	0.832
74	0.727							1.277	1.082
75	0.676							1.813	1.830
76	0.669							1.277	1.082
77	0.698							0.873	0.909
78	0.792							0.958	0.828
79	1.002							0.872	0.905
80	1.093							1.099	1.111

T	Net 21b (N=112)	Net 22 (N=35)	Net 23 (N=54)	Net 24 (N=52)	Net 25 (N=40)	Net 26 (N=54)	Net 27 (N=38)	Net 39 a right (N=88)	Net 39 a left (N=88)
81	1.329							1.872	1.820
82	1.326							1.872	1.820
83	0.987							0.942	1.224
84	0.845							1.567	1.143
85	0.792							1.289	1.289
86	0.789							1.355	1.424
87	0.763							1.812	1.830
88	0.709							1.590	1.589
89	0.746								

TABLE VII. (*Continued.*)

T	Net 21b (N=112)	Net 22 (N=35)	Net 23 (N=54)	Net 24 (N=52)	Net 25 (N=40)	Net 26 (N=54)	Net 27 (N=38)	Net 39 a right (N=88)	Net 39 a left (N=88)
90	0.845								
91	1.055								
92	1.169								
93	1.332								
94	1.363								
95	1.055								
96	1.002								
97	1.093								
98	0.914								
99	0.855								
100	0.887								
101	0.987								
102	1.703								
103	1.169								
104	1.332								
105	1.329								
106	1.187								
107	1.108								
108	1.046								
109	1.623								
110	1.326								
112	1.363								
112	1.703								

[1] R. A. Garza-López and J. J. Kozak, Phys. Rev. E **49**, 1049 (1994).

[2] *Kinetics and Catalysis in Microheterogeneous Systems*, edited by M. Gratzel and K. Kalyanasundarum (Marcel Dekker, New York, 1991); *Photochemistry in Organized and Constrained Media*, edited by V. Ramamurthy (VCH, New York, 1991); *Zeolites and Related Materials: State of the Art*, edited by J. Weitkamp, H. G. Karge, H. Pfeifer, and W. Holderich (Elsevier, New York, 1994); A. J. Bard and M. A. Fox, Acc. Chem. Res. **28**, 141 (1995).

[3] J. J. Kozak, in *Chemical Reactions and Reaction Efficiency in Compartmentalized Systems*, Advances in Chemical Physics Vol. 115, edited by I. Prigogine and Stuart A. Rice (John Wiley & Sons, Inc., New York, 2000), pp. 245–406.

[4] E. W. Montroll, Proc. Symp. Appl. Math. **16**, 193 (1964); E. W. Montroll and G. Weiss, J. Math. Phys. **6**, 167 (1965); E. W. Montroll, *ibid.* **10**, 753 (1969).

[5] R. A. Garza-López, P. Bouchard, G. Nicolis, M. Sleutel, J. Brzezinski, and J. J. Kozak, J. Chem. Phys. **128**, 114701 (2008).

[6] M. O'Keeffe and B. G. Hyde, Philos. Trans. R. Soc. London, Ser. A **295**, 553 (1980).

[7] J. M. Kosterlitz and D. J. Thouless, J. Phys. C **5**, L124 (1972).

[8] B. I. Halperin and D. R. Nelson, Phys. Rev. Lett. **41**, 121 (1978).

[9] D. R. Nelson and B. I. Halperin, Phys. Rev. B **19**, 2457 (1979).

[10] A. P. Young, Phys. Rev. B **19**, 1855 (1979).

[11] D. R. Nelson, in *Phase Transitions and Critical Phenomena*, edited by C. Domb and J. L. Lebowitz (Academic, London, 1983), Vol. 7.

[12] J. J. Kozak, J. Brzezinski, and S. A. Rice, J. Phys. Chem. B **112**, 16059 (2008).

[13] See EPAPS Document No. E-PLEEE8-80-041908 for obtained values for the ratio R upon which the figures in the Appendix are based. For more information on EPAPS, see http://www.aip.org/pubservs/epaps.html.

[14] K. Binder and W. Kob, *Glassy Materials and Disordered Solids* (World Scientific Publishing Co. Pte. Ltd., Singapore, 2005).

[15] Assuming that the triangles in net 22 are equilateral, the set of pentagonal angles that ensure that the sum of angles around any vertex of net 22 is 360° is $[\pi/2$ (twice) and $2\pi/3$ (thrice)]. For this net, neither of the other pentagonal sets of angles identified in [9] satisfies this criterion. Our calculated value for the packing fraction of the unit cell for this net is 0.775 383.

[16] See C. Beta, M. G. Moula, A. S. Mikhailov, H. H. Rotermund, and G. Ertl, Phys. Rev. Lett. **93** 188302 (2004), and articles cited therein.

[17] C. H. Mak, Phys. Rev. E **73**, 065104(R) (2006).